Micro-structured fluid within a channel under static and oscillatory pressure gradients: A novel Darcy-Forchheimer flow investigation

Yijie Li [a], Kashif Ali [b], Sohail Ahmad [b,c], Shahzad Ahmad [c], Wasim Jamshed [d,*], Assmaa Abd-Elmonem [e], Ayesha Amjad [f,g], Sayed M. El Din [h]

[a] School of Computer Science, University of St Andrews, St Andrews KY16 9SX, UK
[b] Department of Basic Science and Humanities, Muhammad Nawaz Sharif University of Engineering & Technology, Multan 60000, Pakistan
[c] Centre for Advanced Studies in Pure & Applied Mathematics, Bahauddin Zakariya University, Multan 60800, Pakistan
[d] Department of Mathematics, Capital University of Science and Technology (CUST), Islamabad 44000, Pakistan
[e] Department of Mathematics, College of Science, King Khalid University, Abha, Saudi Arabia
[f] Faculty of Organization & Management, Silesian University of Technology, 44-100 Gliwice, Poland
[g] Centre for Mechanical Engineering, Materials and Processes (CEMMPRE) University of Coimbra, Polo II, Coimbra 3030-788, Portugal
[h] Center of Research, Faculty of Engineering, Future University in Egypt New Cairo, 11835, Egypt

ARTICLE INFO

ABSTRACT

The pertinence and importance of Darcy-Forchheimer flows can be found in large spectrum of engineering, biological and technological mechanisms like solar absorption and filtration, drainage problems, solar cells, ground stream hydrology, solar panels, irrigation and so forth. The major concern of this study is to interpret that how much a Darcy-Forchheimer flow of a micro-structured fluid (e.g., micropolar fluid) within a channel is influenced by the combined effects of static and oscillatory pressure gradients. Numerical treatment is carried out via three steps explicit Runge-Kutta method. Impacts of the preeminent parameters on the flow, mass and heat transport features of the problem are over looked by means of graphical and tabular representations. The numerical consequences evidently point out that the influence of oscillatory component is to elevate the fluid velocity whereas static component of pressure gradient tends to decelerate the velocity inside the channel. It is also determined here that Darcy parameter sufficiently reduces the angular velocity in the flow regime.

1. Introduction

Micropolar fluids have non-Newtonian nature and possess elements which contain dual nature e.g., micro elements spin and move in a non-symmetric way. This attribute provides a better structure for the effective use of micropolar fluids in modern engineering and technology. These fluids cause a deterioration in the skin friction when interacts with the solid surface. Several fluids like ferro liquids, blood flow in capillaries, polymeric materials, paints, exotic lubricants act as micropolar fluids [1]. The Navier–Stokes equations as described in classical continuum theory are unable to characterize the flow behavior of micropolar fluids at a large scale [2]. It may be attributed from the fact that the Navier–Stokes equations do not comprise of the term which could explain the molecular spin. However, model equations for micropolar fluids involve an additional transport equation from which we can determine the gyration (spin) of micro constituents. The micropolar

fluid theory was explained by Lee et al. [3] and spearheaded by Eringen [4–6]. This work was further flourished and extended by Ariman et al. [7,8].

The micropolar flows, in several geometries, have been interpreted theoretically and numerically by the research community. Vyas et al. [9] investigated radiative micropolar flow through a permeable media taking into account the effect of entropy generation. Fluid motion was caused by a vertically moving infinite plate. Entropy generation got diminished with the impact of heat sink parameter. The micropolar theory was incorporated by Zadravec et al. [10] to formulate the velocity–vorticity relation from Navier–Stokes equations. They employed boundary element method (BEM) to arrange the model equations in integral as well as differential form. Yadav and verma [11] established a mathematical system of equations which expressed the flow of two immiscible fluids one of which was Newtonian fluid and the other was micropolar fluid. An inclined channel having two regions made of two rigid plates was used as geometry. The effects of preeminent parameters on

---

Nomenclature

v_0	wall transpiration velocity, $[ms^{-1}]$
v_B	kinematic viscosity, $[kgm^{-1}s^{-1}]$
v_3	Microrotation, $[MLT^{-1}]$
b	inertial drag coefficient, $[-]$
B	magnetic field, $[Wbm^{-2}]$
T	Temperature, $[K]$
u	horizontal velocity, $[ms^{-1}]$
ρ	density, $[kgm^{-3}]$
k_p	permeability, $[-]$
p	pressure, Pascal
$u1, u2$	velocity components, $[ms^{-1}]$
j	micro-moment of inertia, $[ML^2]$

microrotation and fluid velocity were determined. Kumbinarasaiah and Raghunatha [12] numerically investigated the rotational micropolar fluid flow inside a channel incorporating Parseval frame method. Numerical results, in this paper, were elaborated with the aid of tables and graphs. A study regarding micropolar pulsatile blood flow through an artery was carried out by Shit and Roy [13]. In this paper, impact of magnetic field and body acceleration was taken into account together with heat-transfer characteristics. It was found that wall shear stress reduced with the effect of Hartmann number while heat transfer increased.

Flows through porous medium are eminent in various scientific zones e.g., heat transfer design, geophysics, geothermal processes, catalyst reactions and etc. Modified Darcy flow or the flow through non-Darcian porous medium controls the boundary effects and maintains the temperature distribution. Porous media is beneficial in a wide range of applications including beds of fossil fuels, the motion of water in reservoirs, energy storage units, grain storage, building thermal insulation materials, solar receivers, crude oil production recovery systems, ground water systems, and many more. Contemporary literature reveals that a lot of attention has been given to the flows depicting the involvement of Darcian porous medium. Ganesh et al. [14] numerically investigated the problem of Darcy-Forchheimer flow induced by shrinking/stretching

sheet. The influence of magnetic interaction parameter, viscous and Ohmic dissipation on flow were taken under consideration. The problem of Darcy Forchheimer flow with radiative and convective thermal aspects on micropolar nanofluids in rotating frame of reference was studied by Alzahrani et al. [15]. Raju et al. [16] numerically explored the time dependent nonlinear convective Casson fluid flow over a rotating cone saturated in a porous medium. Shooting technique was employed by Song et al. [17] to investigate the impact of nonlinear thermal radiation and modified Darcy law over micropolar fluid flow across the rotating disk. Impacts of heat source or sink and magnetic field on the Casson nanofluid flow induced by stretching or rorating disk subject to Darcy Forchheimer medium were numerically explored by Siddiqui et al. [18]. Sulochana et al. [19] studied the thermal consequences of MHD nanofluid fluid flow owed by the rotating cone in a resistive porous medium. Analytical solution for the problem of Darcy Forchheimer flow subject to the effects of magnetic dipole over the cone surface was presented by Usman et al. [20].

The eminence of channel flows can be found in a large spectrum to the fields such as circulation of air (modeling) in respiratory system, surface sublimation, combustion process in the rocket motors (as in the case of grain regression), filtration, microfluidic devices, ablation cooling, binary gas diffusion and so on. The focus of this work is to elaborate that how much micro structure of the fluid in a channel is affected by the Darcy-Forchheimer porous medium. The concerned work also presents first effort to deduce the thermal and flow features of the micro structured flow within a channel under the combined effects of stationary and oscillating components of pressure gradient as well as Darcy-Forchheimer medium. The outcomes of the problem are explained via the physical interpretations of graphs and tables.

2. Mathematical formulation of the problem

Micropolar fluid is considered to be flowing through a porous medium which is placed between walls of a channel. The position of the walls is located at $y = \pm d$. The suction is taking place at the upper wall of channel whereas the injection at lower wall. Further, it has been assumed that:

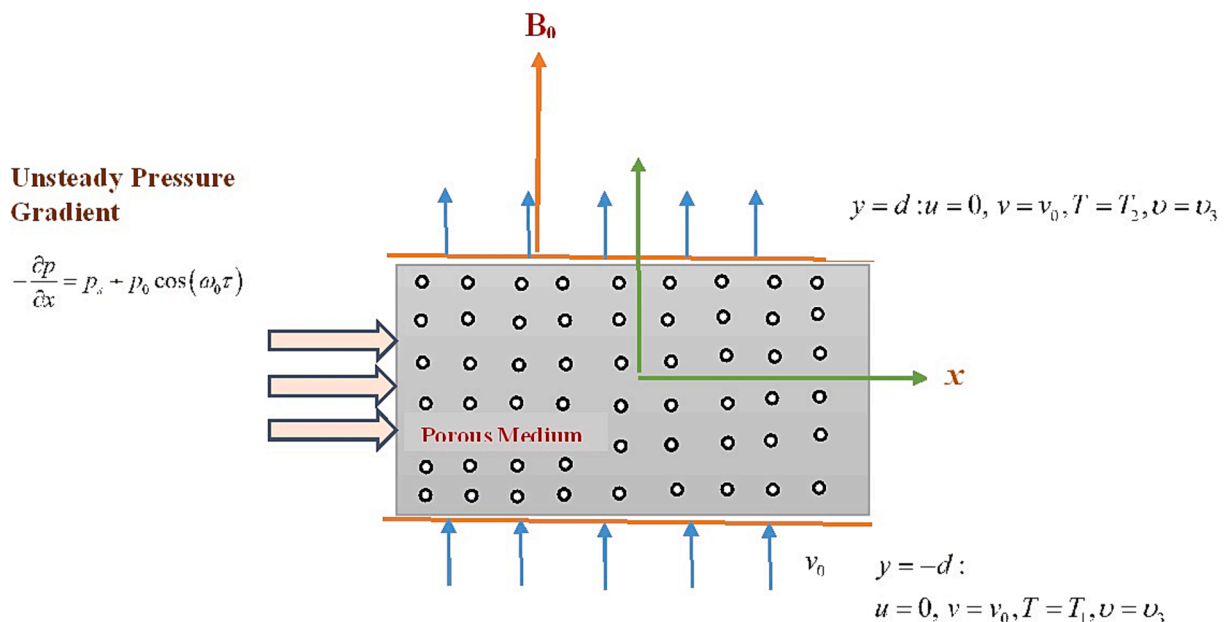- Fluid is flowing due to pressure gradient.

Fig. 1. Geometry of the problem.

- Pressure gradient involves two components e.g., steady and oscillatory.
- Flow is pulsatile and two dimensional.
- Both suction and injection phenomena have been taken into account.
- Non-Darcian porous medium is considered.

The flow geometry is portrayed in Fig. 1.

The model equations for momentum and angular momentum have the form [21,22]:

$$\frac{\partial u}{\partial \tau} + v_o \frac{\partial u}{\partial y} = -\frac{1}{p}\frac{\partial p}{\partial x} + \left(\frac{\mu + k}{\rho}\right)\frac{\partial^2 u}{\partial y^2} + \frac{k}{\rho}\frac{\partial v_3}{\partial y} - \frac{v_B}{k_p}u - bu^2 \tag{1}$$

$$\rho j\left(\frac{\partial v_3}{\partial t} + v_0\frac{\partial v_3}{\partial y}\right) = \gamma\frac{\partial^2 v_3}{\partial y^2} - k\left(\frac{\partial v}{\partial x} - \frac{\partial u}{\partial y}\right) - 2kv_3 \tag{2}$$

Where v_0 and u represent, respectively, the wall transpiration and horizontal velocities. The other terms express: v_B states kinematic viscosity, ρ embodies density, v_3 is used for microrotation, k_p denotes permeability of permeable media, b represents inertial drag coefficient and p exemplifies pressure. It may be important to describe that the Eq. (1) correlates the Forchheimer law and micropolar momentum equation. Last two terms of this equation obey the Forchheimer law. Initially, the micropolar model was spearheaded by Eringen [5,6]. This model was basically based on nonsymmetrical and couple stress tensors. Further details and theory on this topic (micropolar flow b/w channel walls) can be found in our earlier work (Ahmad et al. [23–26]).

Further, it is noted that the horizontal velocity u is the same across every cross section of the channel which means that it does not depend upon the x-coordinate. The continuity equation $\left(\frac{\partial u}{\partial x} + \frac{\partial v}{\partial y} = 0\right)$ therefore takes the form $\frac{dv}{dy} = 0$, which means

$$v = Constant, \tag{3}$$

whereas the wall transpiration condition $(v = v_0 \, at \, y = \pm d)$ transforms the above equation to:

$v = v_0$, everywhere in the channel, which is the reason of appearance of v_0 in the above mathematical model (Eqs. (1)–(2)).

The heat transfer equation can be written as:

$$\frac{\partial T}{\partial \tau} + v_0\frac{\partial T}{\partial y} = \alpha\frac{\partial^2 T}{\partial y^2} \tag{4}$$

Here, the second derivative term is used for thermal diffusion whereas the first derivative term represents thermal convection. The other terms like T and α represent the temperature and thermal diffusivity of the fluid, respectively.

Similarly, the concentration equation may be written as:

$$\frac{\partial C}{\partial \tau} + v_0\frac{\partial C}{\partial y} = D\frac{\partial^2 C}{\partial y^2} - k(C - C_m), \tag{5}$$

with D and k being the mass diffusivity and chemical reaction constant, respectively.

The imposed boundary conditions (BCs) are:

$u = 0, v = v_0, T = T_1, v_3 = 0, C = C_1 \, at \, y = -d$

$u = 0, v = v_0, T = T_2, v_3 = 0, C = C_2 \, at \, y = d \tag{6}$

Whereas the temperatures T_2, T_1 are not same at both (upper and lower) walls. We introduce the non-dimensional parameters such as:

$$U = \frac{v}{v_0}, \xi = \frac{x}{d}, \eta = \frac{y}{d}, t = \frac{v_0}{d}\tau, \tag{7}$$

$$P = \frac{p}{\rho v_0^2}, \theta = \frac{T - T_m}{T_2 - T_m}, \phi = \frac{C - C_m}{C_2 - C_m}, v_3 = \frac{v_0}{d}g(\eta)$$

Table 1a
Parameters of the problem.

$nf = db$	Forchheimer quadratic drag parameter	$C_1 = \frac{k}{\mu}$	Vortex viscosity
$\lambda = \frac{k_{pv_0}}{dv_B}$	Darcy parameter	$Pr = \frac{v_B}{\alpha}$	Prandtl number
$R = \frac{dv_0}{v_B}$	Reynolds number	$C_2 = \frac{d\mu}{\rho jv_0}$	Microinertia density
$C_3 = \frac{\gamma}{d\rho jv_0}$	Spin gradient viscosity	$\gamma = \frac{kd^2}{v_B}$	Chemical reaction parameter

Table 1b
Comparison with velocity $u(\eta)$ on 2nd grid.

η	$u(\eta)$ for 2nd grid (h = 0.01)	
	Ashraf et al. [21]	Present
−0.8	0.447484	0.447595
−0.4	1.014633	1.014744
0	1.212160	1.212271
0.4	1.0655820.496384	1.0656930.496495
0.8		

It is to point out that, only T_1 or T_2 could have been used for obtaining the dimensionless temperature θ, but we have used $\left(T_m = \frac{T_1 + T_2}{2}\right)$ for this purpose, and the similar is true for the dimensionless concentration.

Utilizing the above relations in Eqs. (1), (2), (4) and (5), we achieve following system of equations:

$$\frac{\partial U}{\partial t} + \frac{\partial U}{\partial \eta} = -\frac{\partial P}{\partial \xi} + \left(\frac{1 + C_1}{R}\right)\frac{\partial^2 U}{\partial \eta^2} + \frac{C_1}{R}G'(\eta) - \frac{1}{\lambda}U - NfU^2 \tag{8}$$

$$\frac{\partial G}{\partial t} + G' = C_3 G'' - C_1 C_2\left(\frac{\partial U}{\partial \eta} + 2G\right) \tag{9}$$

$$\frac{\partial \theta}{\partial t} + \frac{\partial \theta}{\partial \eta} = \frac{1}{RPr}\frac{\partial^2 \theta}{\partial \eta^2} \tag{10}$$

$$\frac{\partial \phi}{\partial t} + \frac{\partial \phi}{\partial \eta} = \frac{1}{Sc}\frac{\partial^2 \phi}{\partial \eta^2} - \gamma\frac{1}{R}\phi \tag{11}$$

Parameters involved in the above equations are provided in Table 1. The relation for pressure gradient can be formulated as:

$$-\frac{\partial P}{\partial \xi} = Ps + P0\cos(\omega t) \tag{12}$$

Where Ps and Po express the static and oscillatory pressure gradient components respectively (with frequency ω).

The ultimate BCs with respect to relation (7) take the form:

$\eta = -1 : U = 0, G = 0, \theta = -1, \phi = -1$

$\eta = 1 : U = 0, G = 0, \theta = 1, \phi = 1 \forall t > 0 \tag{13}$

3. Numerical Solution

It is not only difficult to find out the analytical solution of the coupled system (8)-(11) but also it might consume enormous time. However, numerical solution is the choice to obtain the solution to the problem under consideration. For this, we have made use of a fully implicit scheme given below:
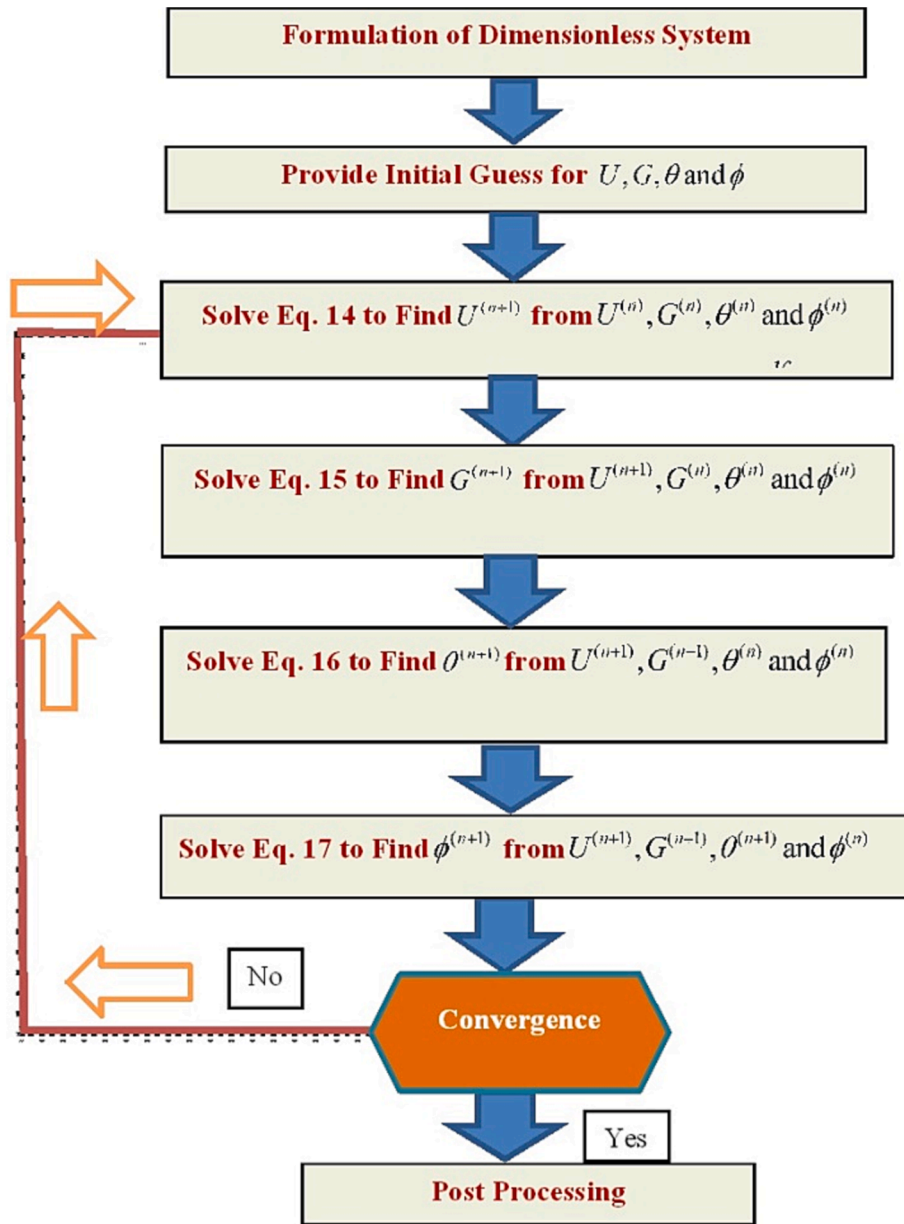
Fig. 2. Flow chart of Computation Procedure.

Table 2
Dimensionless velocity $u(\eta)$ for several values of.

η	$u(\eta)$		
	$h = 0.04$	$h = 0.02$	$h = 0.01$
−1	0	0	0
−0.8	−0.0482	−0.0472	−0.0466
−0.6	−0.0877	−0.0861	−0.0852
−0.4	−0.1183	−0.1162	−0.1151
−0.2	−0.1391	−0.1369	−0.1357
0	−0.1496	−0.1473	−0.1460
0.2	−0.1487	−0.1464	−0.1452
0.4	−0.1349	−0.1329	−0.1317
0.6	−0.1069	−0.1051	−0.1042
0.8	−0.0625	−0.0614	−0.0608
1	0	0	0

$$\frac{U_i^{n+1} - U_i^n}{\delta t} + \frac{U_{i+1}^{n+1} - U_{i-1}^{n+1}}{2\,\delta\eta} = \left\{ P_s + P_0\cos\left(\omega\, t^{(n+1)}\right) \right\} + \frac{1 + C_1}{R}\,\frac{U_{i-1}^{n+1} - 2U_i^{n+1} + U_{i+1}^{n+1}}{(\delta\eta)^2}$$

$$+ \frac{C_1}{R}\,\frac{G_{i+1}^n - G_{i-1}^n}{2\,\delta\eta} - \frac{1}{\lambda}U_i^{n+1} - N_f\left(U_i^{n+1}\right)^2 \tag{14}$$

$$\frac{G_i^{n+1} - G_i^n}{\delta t} + \frac{G_{i+1}^{n+1} - G_{i-1}^{n+1}}{2\,\delta\eta} = C_3\frac{G_{i-1}^{n+1} - 2G_i^{n+1} + G_{i+1}^{n+1}}{(\delta\eta)^2} - C_1 C_2\frac{U_{i+1}^{n+1} - U_{i-1}^{n+1}}{2\,\delta\eta} - 2C_1 C_2 G_i^{n+1} \tag{15}$$

$$\frac{\theta_i^{n+1} - \theta_i^n}{\delta t} + \frac{\theta_{i+1}^{n+1} - \theta_{i-1}^{n+1}}{2\,\delta\eta} = \frac{1}{R\,Pr}\frac{\theta_{i-1}^{n+1} - 2\theta_i^{n+1} + \theta_{i+1}^{n+1}}{(\delta\eta)^2} \tag{16}$$

$$\frac{\phi_i^{n+1} - \phi_i^n}{\delta t} + \frac{\phi_{i+1}^{n+1} - \phi_{i-1}^{n+1}}{2\,\delta\eta} = \frac{1}{Sc}\frac{\phi_{i-1}^{n+1} - 2\phi_i^{n+1} + \phi_{i+1}^{n+1}}{(\delta\eta)^2} - \frac{\gamma}{R}\phi_i^{n+1} \tag{17}$$

At each time step, for every equation, we come across a tridiagonal system which may be solved by using some tridiagonal matrix algorithm (TDMA). Further, as the scheme is fully implicit, it is well known that the step size for obtaining a stable solution is proportional to $\delta\eta$. For the present work, we have obtained the numerical results by taking $\delta t = 0.1\,\delta\eta$. The scientific contributions by Ranocha et al. [27] and Al-Jahdali et al. [28] provide the details on this technique.

Fig. 2 shows the efficiency of the numerical technique used in the present work, as it is clear that the maximum CPU Time for obtaining the numerical solution to the problem for the range of values of the magnetic parameter and the Reynolds number is less than 1 Second. The computations have been made using the same number of grid points and the same value of the time step. Further, there is no monotonic behavior for all values of the two parameters. For example, in case of $Nm = 0, 1, 3$ and 4, the CPU time first drops and then rises as the Reynolds number is increased from R = 1 to R = 5. The trend is however reversed for Nm = 2, and, therefore, any kind of monotonic behavior does not exist.

A numerical data comparison is portrayed in Table 2 which appraises the accuracy of our code. A graphical comparison (see Fig. 2) also validates the code and numerical procedure. The CPU time can be observed from Fig. 3.
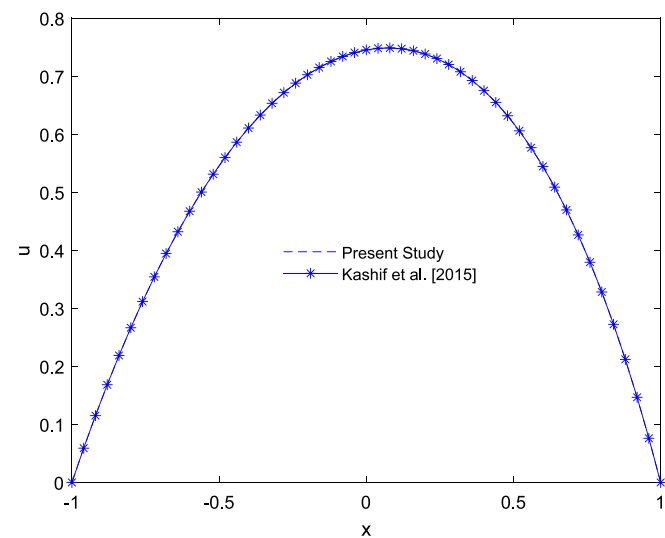
4. Results and discussion

This section depicts our numerical consequences with the help of graphical and tabular representations. The main focus in this study is to determine that how much Darcy Forchheimer porous medium affects the micropolar flow in the coexistence of chemical reaction whereas flow is taken within a channel. The numerical results for microrotation, temperatures, concentration, and velocities are acquired for a wide range of preeminent problem parameters. The values which are used in numerical calculations are specified as:

$\lambda = 0.5$, $C_1 = 1$, $Nf = 0.75$, $R = 0.5$, $Pr = 21$, $C_2 = 0.2$, $P_0 = 1$, $P_s = 2$, $C_3 = 0.3$. In order to validate the code, a comparison for several values of step size η is provided in Table 2. The values of dimensionless velocity $u(\eta)$ seem to be converging in a better way with the increasing values of η. It assures the precision of code to develop the results.

The velocity as well as angular velocity time change across the channel is depicted in Figs. 3 and 4. On the other hand, variation in the temperature and concentration distributions are shown in Figs. 5 and 6. The velocity is noticed to be lower in the first cycle as compared to the corresponding forthcoming cycles. It may be attributed because fluid is at rest initially and when fluid moves then pressure gradient is not enough which could control the velocity that is why velocity increases in the next cycles. High microrotation and velocity is observed near t = o subject to pressure gradient at the stationary fluid (see Figs. 7 and 8). After the first cycle, the upcoming cycles turn towards extension within the channel and finally become periodic. The profiles of isotherms and contours at distinct level of times are illustrated in Figs. 9 and 10. At the beginning when fluid is at rest, temperature seems to be changing in a linear way through channel. But temperature increases and is concentrated near the upper wall of channel when fluid takes a motion (Fig. 11 and Fig. 12).

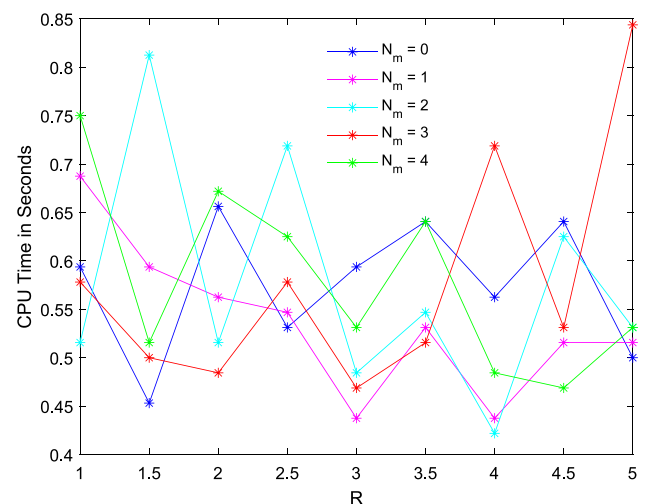In Figs. 6 and 10, we find the dimensionless concentration against

Fig. 2a. Comparison of the Present Results for the Velocity Profile for the Limiting Case of Newtonian Fluid without any Solid Nano Particles (see Kashif et al. [22]).

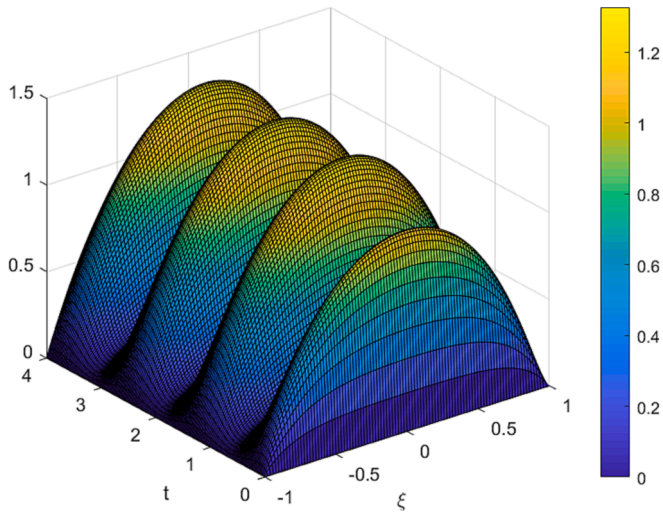**Fig. 2b.** Variation in the CPU Time with the Reynolds Number R.

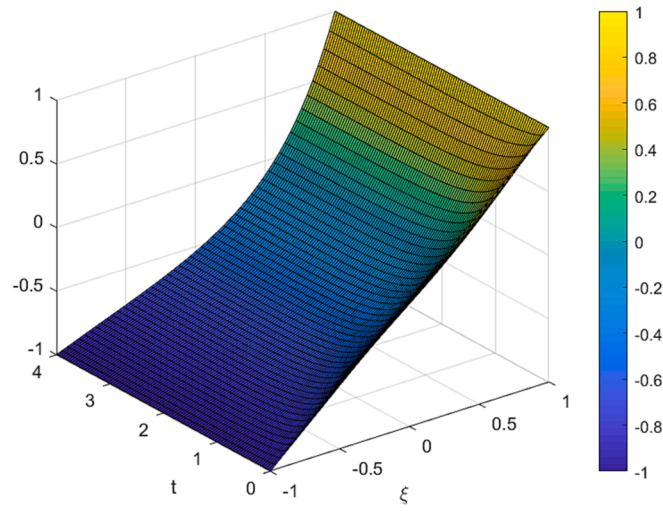**Fig. 3.** Change in the velocity field with time.

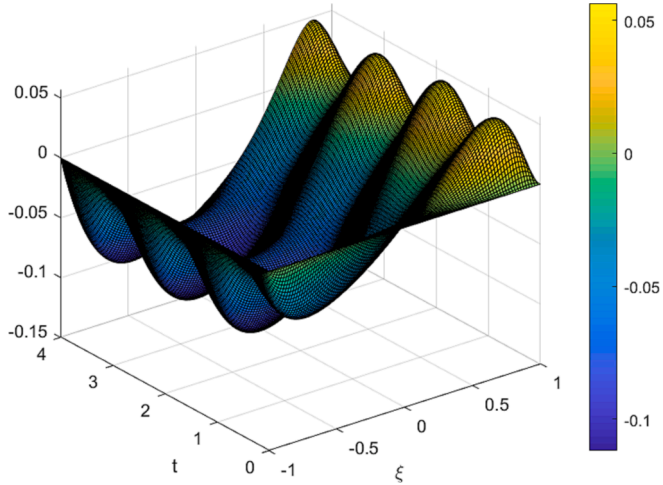**Fig. 6.** Change in the concentration with time.

Fig. 4. Change in the microrotation with time.
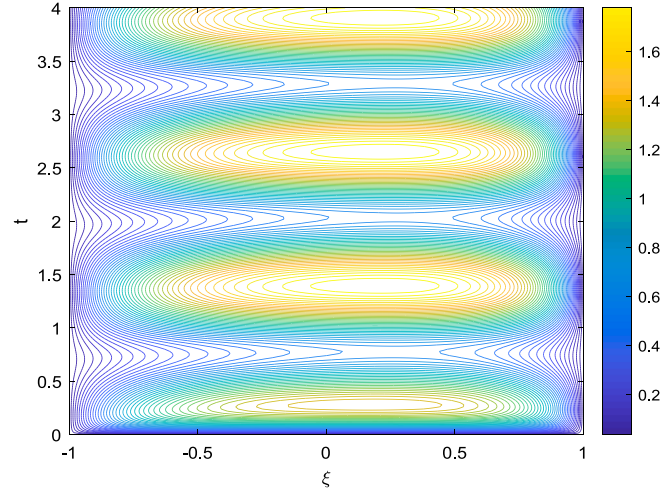

Fig. 7. Velocity contours at different time levels.
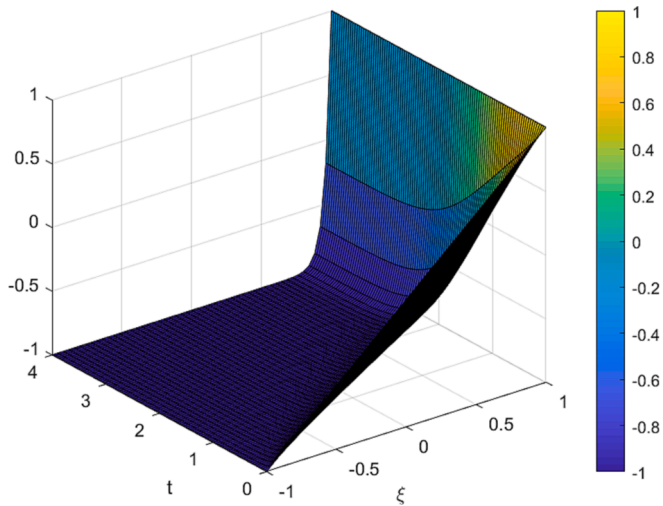

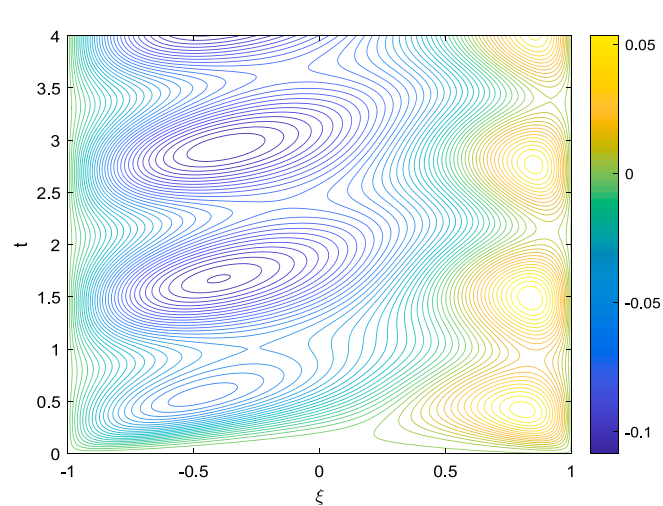**Fig. 5.** Change in the temperature with time.

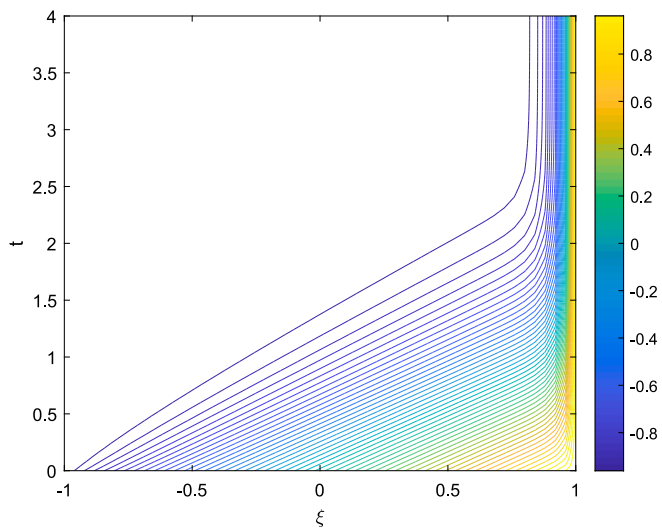**Fig. 8.** Micro-rotation contours at different time levels.
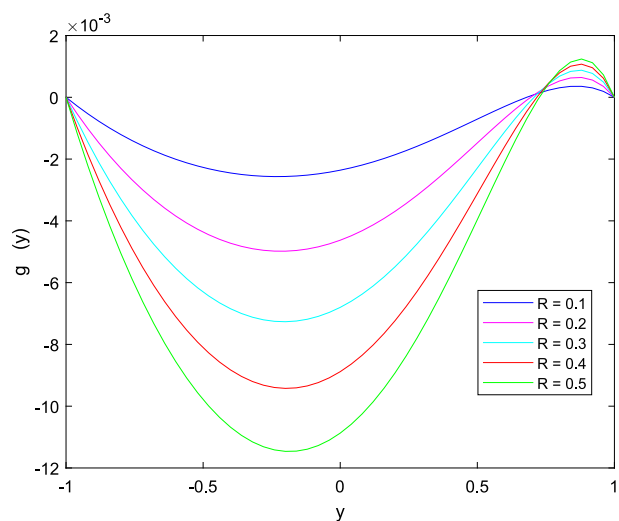
Fig. 9. Isotherms at different time levels.

Fig. 10. Contours of the concentration field at different time levels.

Fig. 11. Impact of the Reynolds number on the velocity profile.

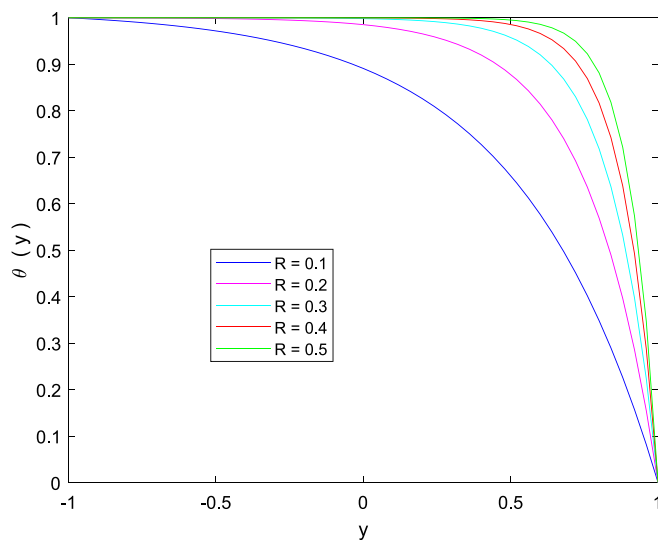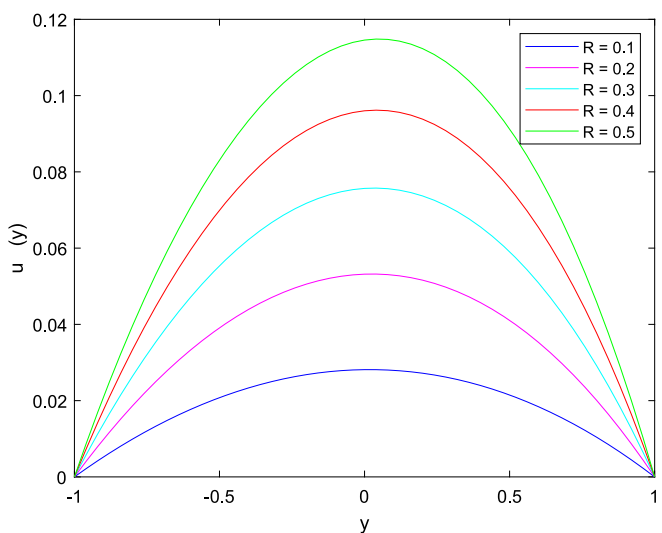**Fig. 12.** Impact of the Reynolds number on the microrotation profile.

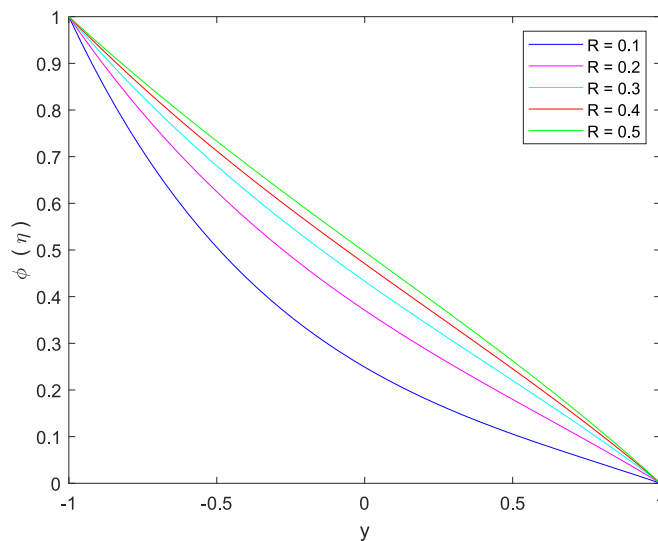**Fig. 13.** Impact of the Reynolds number on the temperature profile.

Fig. 14. Impact of the Reynolds number on the concentration profile.

Fig. 15. Impact of the Darcy parameter on the velocity profile.

Fig. 16. Impact of the Darcy parameter on the microrotation profile.

Fig. 17. Impact of the Forchheimer quadratic drag parameter on the velocity profile.
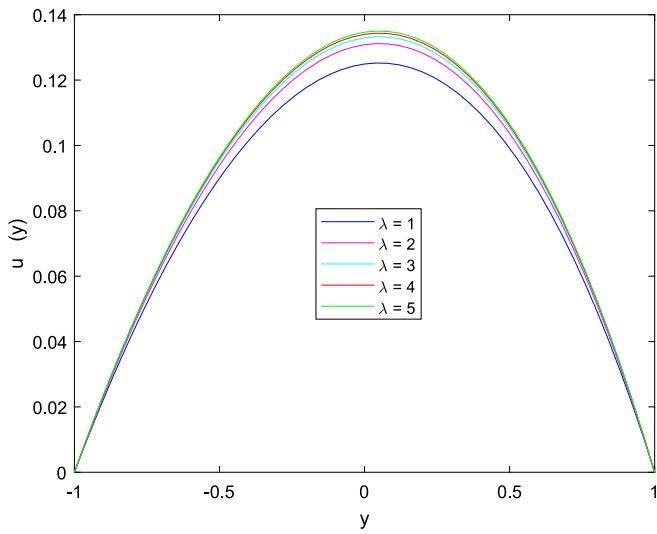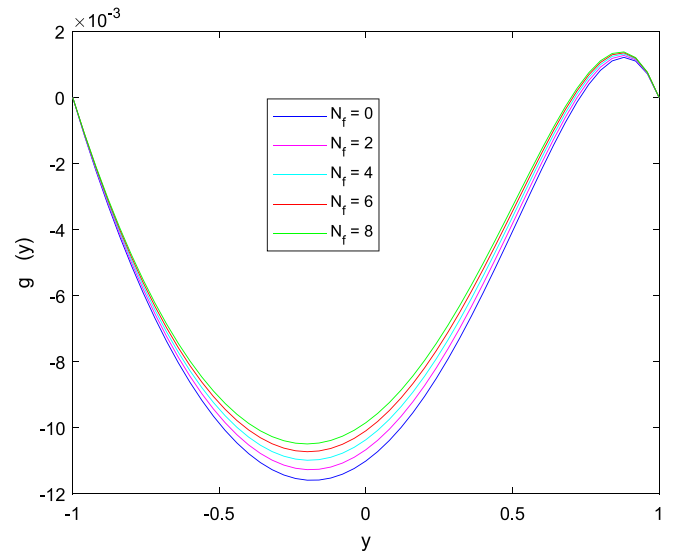

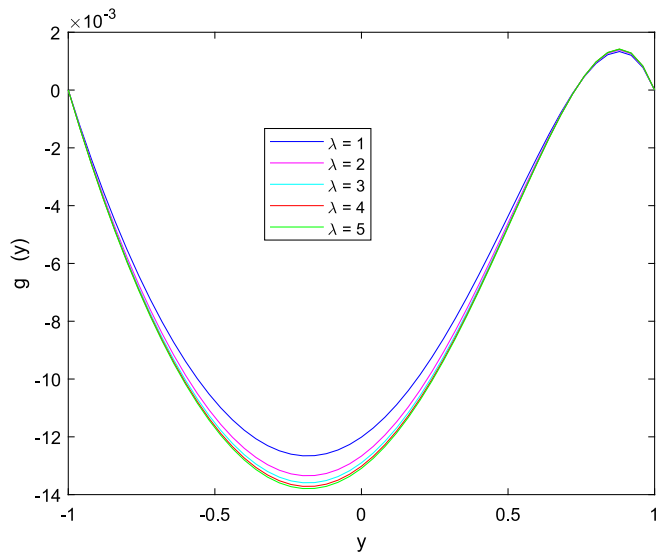**Fig. 18.** Microrotation profile against Forchheimer quadratic drag parameter.
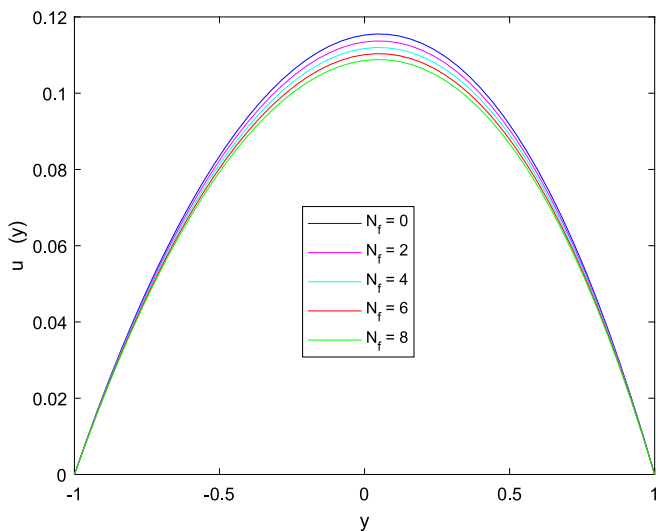

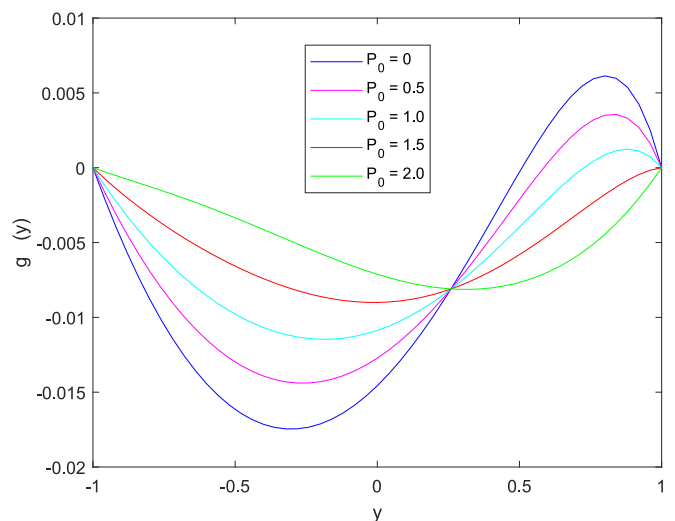**Fig. 19.** Velocity profile against static component of pressure gradient.

Fig. 20. Microrotation profile against static component of pressure gradient.
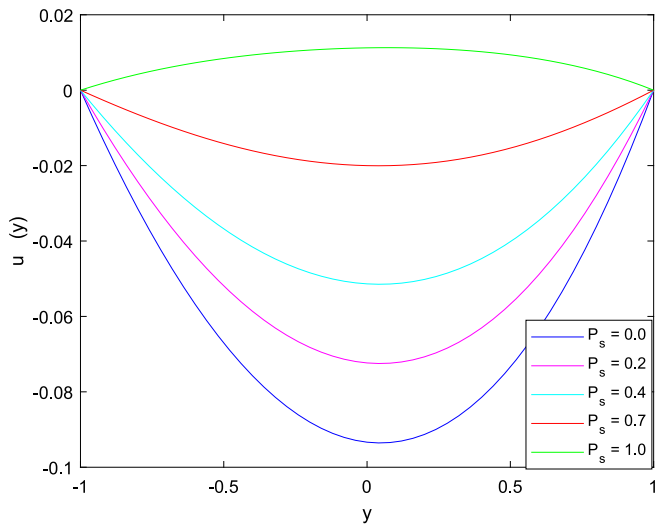
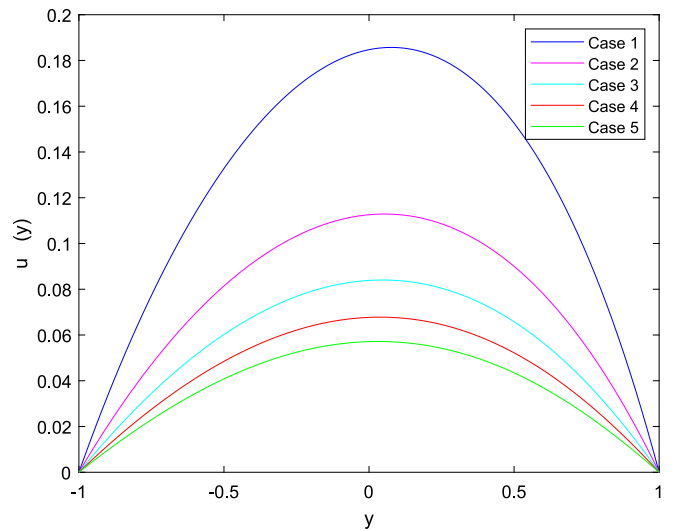**Fig. 21.** Velocity profile against oscillatory component of pressure gradient.

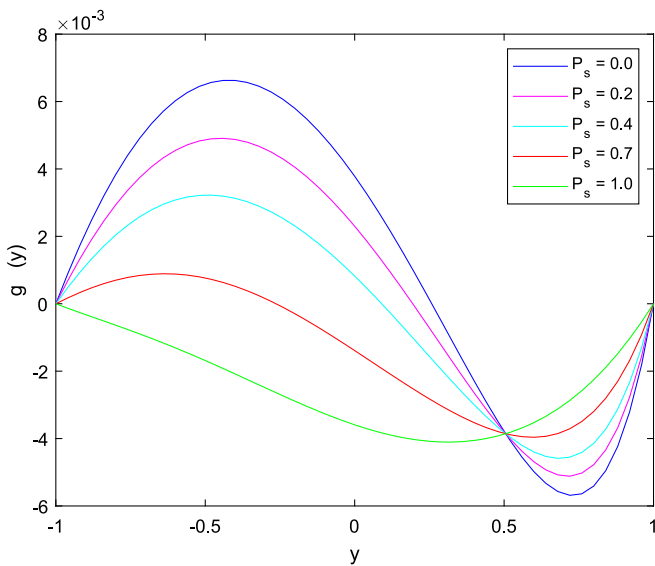**Fig. 23.** Velocity profile against material parameters.

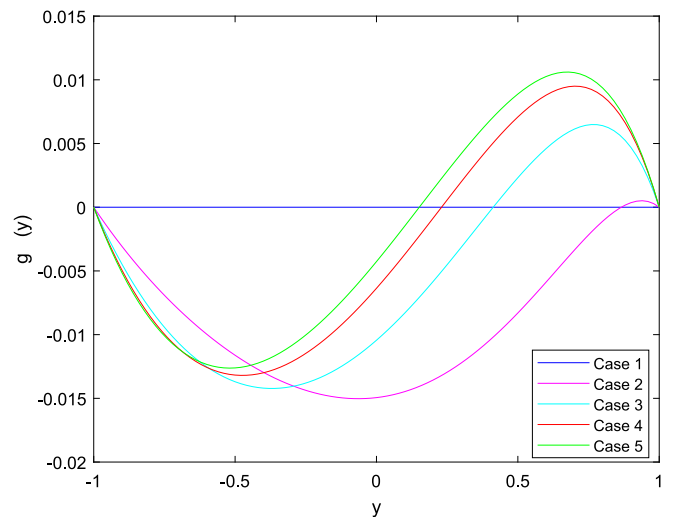**Fig. 22.** Microrotation profile against oscillatory component of pressure gradient.

Fig. 24. Microrotation profile against material parameters.

Table 3
Five cases of micropolar parameters.

Cases	C_1	C_2	C_3
1st case	0.0	0.0	0.0
2nd case	0.6	0.2	0.2
3rd case	1.2	0.4	0.4
4th case	1.8	0.6	0.6
5th case	2.4	0.8	0.8

the dimensionless time. The linearity is due to the relatively lower values of the chemical reaction parameter γ. We have checked that the linear nature of the concentration distribution is distorted if the parameter is raised.

It is noticed that the fluid is accelerated across the channel with the effect of transpiration Reynolds number R (please see Fig. 13). Fig. 14 shows the variation in the concentration profile with the Reynolds number (R). We note the presence of the factor ($1/R$) with the chemical reaction term in the governing equation for concentration (Eq. (11)). Consequently, as R is raised, the impact of chemical reaction on the profile is reduced, and therefore we note shift in the qualitative behavior of the graph. That is, its nature changes from nonlinear to linear one. Temperature and concentration seem to be deteriorating by the Reynolds number across the flow regime. The impact of Darcy parameter λ on dimensionless velocity and microrotation is depicted in Figs. 15 and 16. An increase in the levels of λ may cause a decrement in the Darcian drag force (which is denoted by the factor $-\frac{U}{\lambda}$ in eq. (1)). Due to this attribute, flow faces less resistance which causes acceleration in the micropolar fluid. However, the cumulative impact of λ tends to speed up

the flow within the channel, as depicted in Fig. 15. On the other hand, angular velocity profile falls almost at the center of channel (Fig. 16). From the figure, we also note that microrotation is negative in major part of the domain, thereby meaning that micro scaled particles are spinning in clockwise direction here. But there is also a smaller part near the upper channel wall where the particles are spinning in anti-clockwise direction. So, considering the magnitude of microrotation (which is the strength with which the particles are spinning), the maxima lies nearly at $y = -0.2$ which in turn means that this is the location where the particles are spinning most intensely. The increasing values of Forchheimer quadratic drag parameter Nf (this term is represented by $-NfU^2$ in Eq. (6)) would resist the flow due to which fluid velocity

reduces, as elucidated in Fig. 17. The Forchheimer parameter Nf substantially upsurge the angular velocity across the channel (as appeared in Fig. 18) whereas Darcy parameter λ generate opposite effect on microrotation as equated to the parameter Nf.

Figs. 19-22 interpret the impact of static as well as oscillatory component of pressure gradients (and respectively) on dimensionless velocities and microrotations. It can be evidently examined from these diagrams that both parameters generate opposite effects such that velocity is reduced by the static component of pressure gradient and enhanced by the oscillatory component of pressure gradient. In the same way, microrotation accelerates initially with the effect of pressure gradient but it decelerates gradually near the upper wall of channel just after concavity. It is important to note that the driving force for present flow problem is the pressure gradient whose magnitude is determined by static and oscillatory components and. From Fig. 20, it is interesting to note that the static pressure gradient tends to suppress the spinning (both the clockwise and anticlockwise) of the particles. The oscillatory component of pressure gradient yields almost opposite effect on angular velocity as equated to the static component of pressure gradient. We have taken five cases of the material parameters to analyze their effects on dimensionless microrotation and velocity. It is examined here that both velocity and microrotation got decelerated with the influence of parameters C_1, C_2 and C_3 which are micropolar parameters (see Figs. 23 and 24). The values which have been used for various cases of material parameters are depicted in Table 3. The role of several parameters on the efficiency of fluid dynamics is further elaborated in refs. [29–39].

5. Conclusions

An inclusive analysis of micropolar flow under the simultaneous effects of static and oscillatory pressure gradients is presented in the concerned work. Numerical solution is determined by utilizing a fully implicit numerical scheme. Flow and thermal features of the problem are analyzed for the prominent effects of the problem parameters. The main consequences can be described as:

- The impact of Darcy parameter tends to speed up the flow within the channel whereas Forchheimer quadratic drag parameter resists the flow due to which fluid velocity reduces
- The Reynolds number causes a deceleration in the microrotation but accelerates the velocity.
- The microrotation accelerates initially with the effect of pressure gradient P_0 but after concavity it decelerates gradually near the upper wall of channel.
- Both the oscillatory and static components of pressure gradient yield opposite effect to each other, in case of their effects, on velocity and concentration.

Declaration of Competing Interest

The authors declare that they have no known competing financial interests or personal relationships that could have appeared to influence the work reported in this paper.

Acknowledgments

References

[1] S. Ahmad, M. Ashraf, K. Ali, K.S. Nisar, Computational analysis of heat and mass transfer in a micropolar fluid flow through a porous medium between permeable channel walls, Int. J. Nonlinear Sci. Numer. Simul. (2021), https://doi.org/10.1515/ijnsns-2020-0017.

[2] S. Ahmad, K. Ali, S. Ahmad, J. Cai, Numerical study of Lorentz force interaction with micro structure in channel flow, Energies 14 (2021) 4286, https://doi.org/10.3390/en14144286.

[3] J. Lee, X. Wang, J. Chen, An overview of micromorphic theory in multiscaling of synthetic and natural systems with self-adaptive capability, National Taiwan University of Science and Technology Press, Taipei, Taiwan, 2010, pp. 81–84.

[4] A.C. Eringen, Simple microfluids, Int. J. Eng. Sci. 2 (2) (1964) 205–217.

[5] A. Eringen, Theory of micropolar fluids, J. Math. Mech. 16 (1) (1966) 1–18.

[6] A.C. Eringen, Theory of thermomicrofluids, J. Math. Anal. Appl. 38 (2) (1972) 480–496.

[7] T. Ariman, M.A. Turk, N.D. Sylvester, Microcontinuum fluid mechanics—a review, Int. J. Eng. Sci. 11 (8) (1973) 905–930.

[8] T. Ariman, M.A. Turk, N.D. Sylvester, Applications of microcontinuum fluid mechanics, Int. J. Eng. Sci. 12 (4) (1974) 273–293.

[9] P. Vyas, R.K. Kasana, S. Khan, Entropy analysis for boundary layer micropolar fluid flow, AIMS Math. 5 (3) (2020) 2009–2026, https://doi.org/10.3934/math.2020133.

[10] M. Zadravec, M. Hriberšek, L. Škerget, Micropolar fluid flow modelling using the boundary element method, Comput. Methods Multiphase Flow IV 56 (8) (2007) 325–332.

[11] P.R. Yadav, A.K. Verma, Analysis of two immiscible Newtonian and micropolar fluid flow through an inclined porous channel, Math. Methods Appl. Sci. 45 (3) (2022) 1701–1724.

[12] S. Kumbinarasaiah, K.R. Raghunatha, A novel approach on micropolar fluid flow in a porous channel with high mass transfer via wavelet frames, Nonlin. Eng. 10 (2021) 39–45.

[13] G.C. Shit, M. Roy, Pulsatile flow and heat transfer of a magneto-micropolar fluid through a stenosed artery under the influence of body acceleration, J. Mech. Med. Biol. 11 (3) (2011) 643–661.

[14] N.V. Ganesh, A.K.A. Hakeem, B. Ganga, Darcy-Forchheimer flow of hydromagnetic nanofluid over a stretching/shrinking sheet in a thermally stratified porous medium with second order slip, viscous and Ohmic dissipations effects, Ain Shams Eng. J. 9 (4) (2018) 939–951, https://doi.org/10.1016/j.asej.2016.04.019.

[15] E.O. Alzahrani, Z. Shah, W. Alghamdi, M.Z. Ullah, Darcy-Forchheimer radiative flow of micropolar CNT nanofluid in rotating frame with convective heat generation/consumption, Process. Fluid Flow Heat Transf. Nanofluids 7 (10) (2019) 666, https://doi.org/10.3390/pr7100666.

[16] A.B.M.M. Raju, G.S.S. Raju, B. Mallikarjuna, C.S.K. Raju, Effects of nonlinear convection and variable properties on Darcy flow of non-Newtonian fluid over a rotating cone, Int. J. Res. Eng. Applic. Manag. 4 (2) (2018), https://doi.org/10.18231/2454-9150.2018.0270.

[17] Y.Q. Song, S.A. Khan, M. Imran, H. Waqas, S.U. Khan, M.I. Khan, S. Qayyum, Y.M. Chu, Applications of modified Darcy law and nonlinear thermal radiation in bioconvection flow of micropolar nanofluid over an off centered rotating disk, Alex. Eng. J. 60 (5) (2021) 4607–4618.

[18] B.K. Siddiqui, S. Batool, M.Y. Malik, Q.M. Hassan, A.S. Alqahtani, Darcy Forchheimer bioconvection flow of Casson nanofluid due to a rotating and stretching disk together with thermal radiation and entropy generation, Case Stud. Therm. Eng. 27 (2021), 101201, https://doi.org/10.1016/j.csite.2021.101201.

[19] C. Sulochana, G.P. Ashwinkumar, N. Sandeep, Numerical investigation of chemically reacting MHD flow due to a rotating cone with thermophoresis and brownian motion, Int. J. Adv. Sci. Technol. 86 (2016) 61–74, https://doi.org/10.14257/ijast.2016.86.06.

[20] A.H. Usman, Z. Shah, P. Kumam, W. Khan, U.W. Humphries, Nanomechanical concepts in magnetically guided systems to investigate the magnetic dipole effect on ferromagnetic flow past a vertical cone surface, Coatings 11 (9) (2021) 1129, https://doi.org/10.3390/coatings11091129.

[21] M. Ashraf, K. Ali, M.M. Ashraf, Numerical simulation of micropolar flow in a channel under oscillatory pressure gradient, Iran. J. Chem. Chem. Eng. 39 (2020) 263–272.

[22] K. Ali, S. Ahmad, S. Ahmad, et al., On the interaction between the external magnetic field and nanofluid inside a vertical square duct, AIP Adv. 5 (2015) 107120.

[23] S. Ahmad, M. Ashraf, K. Ali, Numerical simulation of viscous dissipation in a micropolar fluid flow through a porous medium, J. Appl. Mech. Tech. Phys. 60 (6) (2019) 996–1004, https://doi.org/10.1134/S0021894419060038.

[24] S. Ahmad, M. Ashraf, K. Ali, Simulation of thermal radiation in a micropolar fluid flow through a porous medium between channel walls, J. Therm. Anal. Calorim. 144 (3) (2021) 941–953, https://doi.org/10.1007/s10973-020-09542-w.

[25] K.S. Nisar, A.A. Faridi, S. Ahmad, N. Khan, K. Ali, W. Jamshed, A.-H. Abdel-Aty, I.S. Yahia, Cumulative impact of micropolar fluid and porosity on MHD channel flow: a numerical study, Coatings 12 (1) (2022) 93.

[26] K. Ali, S. Ahmad, M. Ashraf, Numerical simulation of MHD pulsatile flow of a biofluid in a channel, AIP Adv. 5 (2015) 087130.

[27] H. Ranocha, L. Dalcin, M. Parsani, D.I. Ketcheson, Optimized Runge-Kutta methods with automatic step size control for compressible computational fluid dynamics, Commun. Appl. Math. Comput. 4 (4) (2022) 1191–1228.

[28] R. Al Jahdali, L. Dalcin, M. Parsani, On the performance of relaxation and adaptive explicit Runge-Kutta schemes for high-order compressible flow simulations, J. Comput. Phys. 464 (2022) 111333.

[29] S. Das, N. Mahato, A. Ali, R.N. Jana, Aspects of Arrhenius kinetics and Hall currents on gyratory Couette flow of magnetized ethylene glycol containing bi-hybridized nanomaterials, Heat Transf. 52 (4) (2023) 2995–3026.

[30] S. Das, B. Tarafdar, B.C. Sarkar, R.N. Jana, Rotational magneto-hydrodynamic Couette flow of nanofluids with hall effects, J. Nanofluids 8 (3) (2019) 604–619.

[31] M.G. Reddy, K.G. Kumar, Cattaneo-Christov heat flux feature on carbon nanotubes filled with micropolar liquid over a melting surface: a stream line study, Int. Commun. Heat Mass Transf. 122 (2021) 105142.

[32] S. Sureshkumar Raju, K. Ganesh Kumar, M. Rahimi-Gorji, I. Khan, Darcy-Forchheimer flow and heat transfer augmentation of a viscoelastic fluid over an incessant moving needle in the presence of viscous dissipation, Microsyst. Technol. 25 (9) (2019) 3399–3405.

[33] M. Gnaneswara Reddy, M.V.V.N.L. Sudharani, K. Ganesh Kumar, A.J. Chamkha, G. Lorenzini, Physical aspects of Darcy-Forchheimer flow and dissipative heat transfer of Reiner-Philippoff fluid, J. Therm. Anal. Calorim. 141 (2) (2020) 829–838.

[34] M.G. Reddy, P. Vijayakumari, K.G. Kumar, S.A. Shehzad, Zero-mass flux and Cattaneo-Christov heat flux through a Prandtl non-Newtonian nanofluid in Darcy-Forchheimer porous space, Heat Transf. 50 (1) (2021) 220–233.

[35] K.G. Kumar, A.J. Chamkha, Darcy-Forchheimer flow and heat transfer of water-based Cu nanoparticles in convergent/divergent channel subjected to particle shape effect, Eur. Phys. J. Plus 134 (2019) 107, https://doi.org/10.1140/epjp/i2019-12447-y.

[36] K. Ganesh Kumar, M.G. Reddy, M.I. Khan, F. Alzahrani, M.I. Khan, E.R. El-Zahar, Heat transfer and melting flow of a Reiner-Philippoff fluid over a surface with Darcy-Forchheimer medium, Case Stud. Therm. Eng. 28 (2021) 101649.

[37] M.R. Eid, W. Jamshed, B.S. Goud, R.W. Usman, S.M. El Ibrahim, A.-E. Din, N. S. Elmki Abdalla, Mathematical analysis for energy transfer of micropolar magnetic viscous nanofluid flow on permeable inclined surface and Dufour impact, Case Stud. Therm. Eng. 49 (2023), 103211.

[38] T. Sajid, W. Jamshed, S. Algarni, T. Alqahtani, M.R. Eid, K. Irshad, G. C. Altamirano, S.M. El Din, K.W. Nahar Tajer, Catalysis reaction influence on 3D tetra hybrid nanofluid flow via oil rig solar panel sheet: Case study towards oil extraction, Case Stud. Therm. Eng. 49 (2023), 103296.

[39] F. Wang, T. Sajid, N.M. Katbar, W. Jamshed, M.R. Usman, A. Eid, S.S. Abd-Elmonem, S.M. El Putri Mohamed Isa, A.A. Din, G.C. Altamirano, Computational examination of non-Darcian flow of radiative ternary hybridity Casson nanoliquid through moving rotary cone, J. Comput. Des. Eng. (2023).